Journal of Materials Chemistry C

ROYAL SOCIETY OF CHEMISTRY

PAPER

View Article Online
View Journal | View Issue

Cite this: J. Mater. Chem. C, 2020, 8, 15175

Design of narrow bandgap non-fullerene acceptors for photovoltaic applications and investigation of non-geminate recombination dynamics†

Joachim Vollbrecht,[a] Jaewon Lee,[ab] Seo-Jin Ko,[c] Viktor V. Brus,[a] Akchheta Karki,[a] William Le,[a] Martin Seifrid,[a] Michael J. Ford,[a] Kilwon Cho,[d] Guillermo C. Bazan[a] and Thuc-Quyen Nguyen*[a]

Received 1st May 2020,
Accepted 1st July 2020

DOI: 10.1039/d0tc02136a

rsc.li/materials-c

A new narrow bandgap non-fullerene electron acceptor was designed, synthesized, and characterized for near-infrared organic photovoltaics. This acceptor was compared to a structurally similar compound with systematically modified side chains, and a series of solar cells were fabricated, employing the common donor polymers PTB7-Th and PBDBT. The devices exhibited charge generation over a wide spectral range and power conversion efficiencies up to 8.1%. The non-geminate recombination dynamics were investigated and quantified *via* a combination of capacitance spectroscopy and transient open-circuit voltage decay measurements. The reduction of the bandgap results in increased bimolecular recombination losses, while solar cells composed of PBDBT were afflicted by stronger monomolecular, *i.e.* trap-assisted, recombination losses that ultimately caused the lower power conversion efficiencies of the respective devices. The latter observation could be correlated to less ordered blend film morphology.

1. Introduction

In recent years, organic photovoltaics (OPVs) have received increasing attention owing to the potential of manufacturing large-area, flexible solar cells *via* mild and economically favorable solution-based processing techniques.[1,2] The gains in performance recently observed for OPVs can mostly be attributed to the use of non-fullerene acceptors (NFAs) that were developed through continuous efforts to replace the hitherto ubiquitous fullerene-based acceptors.[3,4] Organic solar cells (OSCs) based on fullerene acceptors in a bulk-heterojunction (BHJ) configuration yield power conversion efficiencies (PCEs) of up to 11% for single-junction devices,[5,6] while PCEs of over 17% have been reported for state-of-the-art, single-junction and tandem NFA-OSCs, placing them within reach of the performance range of perovskite solar cells.[7–9] In addition to the increased performance, NFAs can be tuned to yield compounds that absorb at longer wavelengths (*e.g.*, near-infrared).[10,11] This control over the bandgap opens up the potential to develop semi-transparent OSCs that could find application in building-integrated photovoltaics and in agriculture.[12,13] Even when considering the recent advances in NFAs, it is still necessary to develop a deeper understanding of loss mechanisms in NFAs such as non-radiative and non-geminate recombination – the process where free electrons and holes originating from different excitons recombine – to further improve the performance of OSCs.[14–18] This is especially required since the interplay between narrow bandgap NFAs ($E_g \leq 1.3$ eV) and polymers such as PTB7-Th or PBDBT, originally designed for fullerene acceptors,[19,20] is yet not fully understood.[21,22] Hence, this study focuses on four different narrow bandgap blend systems in solar cells, the observed photo-physical, morphological, and OPV performance differences, and how these differences relate to the non-geminate recombination dynamics.

2. Results and discussion

We recently reported narrow bandgap electron acceptors, namely CTIC-4F and COTIC-4F, which are characterized by

[a] Center for Polymers and Organic Solids, Departments of Chemistry and Biochemistry, University of California at Santa Barbara, Santa Barbara, CA 93106, USA. E-mail: quyen@chem.ucsb.edu
[b] Department of Chemical Engineering and Applied Chemistry, Chungnam National University, Daejeon, 34134, Republic of Korea
[c] Division of Advanced Materials, Korea Research Institute of Chemical Technology (KRICT), Daejeon 34114, Republic of Korea
[d] Center for Advanced Soft Electronics, Department of Chemical Engineering Pohang, University of Science and Technology, Pohang, 37673, Republic of Korea

† Electronic supplementary information (ESI) available: Additional details about the synthesis, characterization, device fabrication, experimental setups, recombination analysis, and morphological measurements are provided in the supporting information. See DOI: 10.1039/d0tc02136a

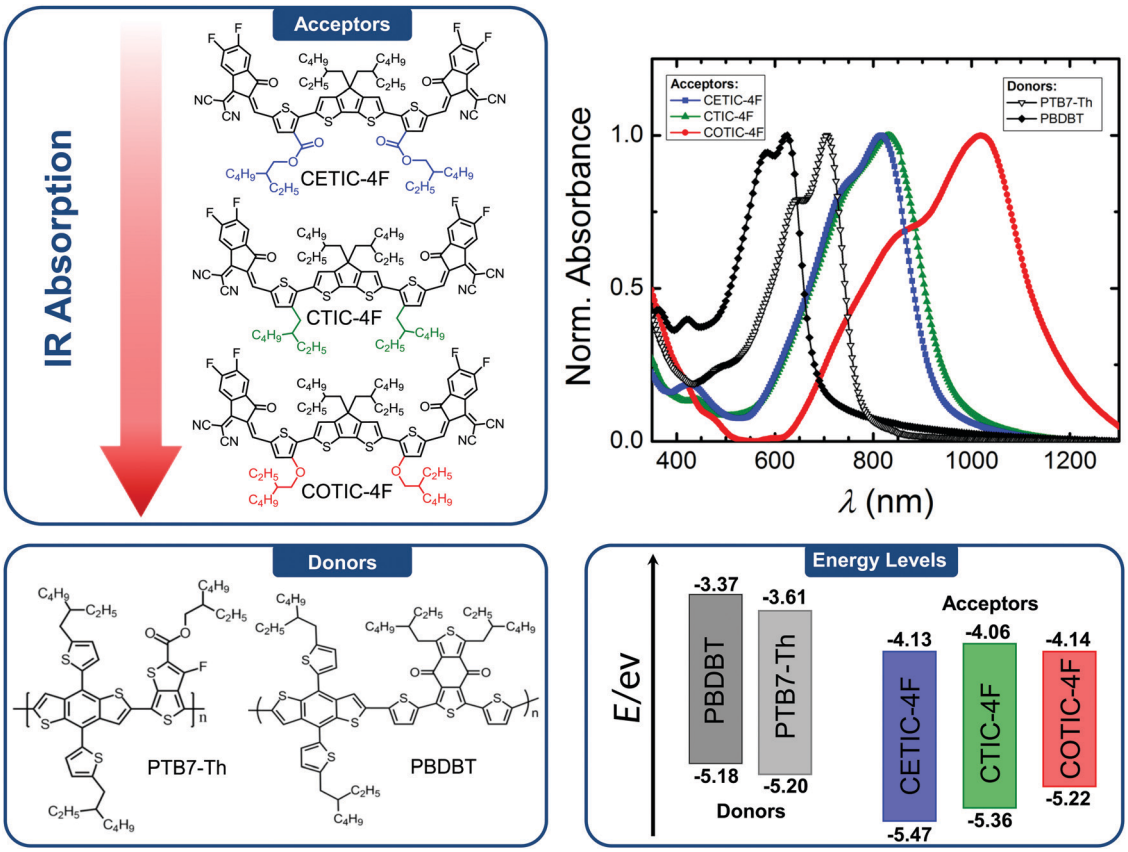

Fig. 1 Chemical structures of the studied non-fullerene acceptors and donor polymers, absorption spectra of pristine thin films, and relevant energy levels. The chemical structure, absorption spectrum, and relevant energy levels of CTIC-4F are depicted for reference.

optical bandgaps (E_g^{opt}) of 1.3 and 1.1 eV, respectively.[11,23] The molecules are designed based on an A–D′–D–D′–A molecular configuration, consisting of cyclopentadithiophene (CPDT) as the central donor (D) unit, thienyl units as the flanked sub-donor (D′) fragments, and 2-(5,6-difluoro-3-oxo-2,3-dihydro-1*H*-inden-1-ylidene)malononitrile as the terminal acceptor (A) units. The molecular structures of CTIC-4F and COTIC-4F differ by their side chains on the D′ fragments, specifically alkyl *vs.* alkoxy groups for CTIC-4F *vs.* COTIC-4F. Changing the substituent of side chains on the thienyl fragments is an effective way to modulate the frontier orbital energy levels and absorption profiles of organic semiconductors.[24,25] In this work, we designed a new NFA derivative, namely CETIC-4F (Fig. 1), containing an ester substituted group in the 3-position of the D′–thienyl unit (see Scheme S1 and Fig. S1–S4, ESI†). As evidenced by the optical transitions and the cyclic voltammetry, incorporating electron-withdrawing ester substituents into alkyl side chains lowers the HOMO level from −5.36 eV for CTIC-4F to −5.47 eV for CETIC-4F, while resulting in a minor effect on the optical bandgap (Fig. 1 and Fig. S7, ESI†). These experimental results were further confirmed by employing quantum chemical calculations based on density functional theory (DFT). It was revealed that the side chains play an important role in the energy levels of the compounds; first, due to their different electron-donating properties and, second, due to the different backbone planarity of the studied compounds resulting from the alkoxy and ester groups in the side chains (Fig. S8 and S9, ESI†).

This underlines the potential of the aforementioned synthetic strategy to finely tune the NFAs for energy level matching, while maintaining a similar bandgap.

Organic solar cells were fabricated and optimized to investigate the photovoltaic performance of two donors and two NFAs, namely PBDBT and PTB7-Th[19,20,26] as well as CETIC-4F and COTIC-4F (see ESI†).[11,23] The same trend in performance can be observed for the two sets of devices with different donors, where of the investigated NFAs, CETIC-4F shows the highest PCE compared to COTIC-4F (see Fig. 2 and Table 1). Furthermore, the devices with PTB7-Th as the donor perform better than their PBDBT counterparts, owing to higher values of the short-circuit current density (J_{SC}) and fill factor (FF), while in contrast the open-circuit voltages (V_{OC}) tend to be of a similar value. The COTIC-4F devices showed the biggest drop in PCE when changing the donor polymer, namely from up to 7.04% (PTB7-Th:COTIC-4F) to only 2.32% (PBDBT:COTIC-4F). The external quantum efficiency (EQE) measurements reveal that PTB7-Th:CETIC-4F and PBDBT:CETIC-4F devices show charge carrier generation in the spectral range of 300–950 nm, while PTB7-Th:COTIC-4F and PBDBT:COTIC-4F devices exhibit charge generation at even longer wavelengths (300–1100 nm), which is in good agreement with the thin film absorption spectra and earlier reports (Fig. 1 and 2).[11] Furthermore, the

photocurrent density (J_{ph}) was calculated, which is defined as follows:

$$J_{ph} = J_{light} - J_{dark}, \quad (1)$$

where J_{light} is the current density under illumination and J_{dark} is the current density in the dark (see Fig. S13–S15, ESI†). The photocurrent density can be compared between the different devices by plotting against the effective voltage $V_{eff} = V_0 - V_{cor}$, where V_0 is the voltage at which $J_{ph} = 0$ (Fig. 2) and V_{cor} is the applied voltage corrected for the losses caused by the series resistance ($V_{cor} = V_{app} - J \cdot R_{series}$).[27,28] Similarly, the probability of charge collection P_C is accessible from the ratio between the saturated photocurrent density $J_{ph,sat}$ with the values for J_{ph} at different biases:[29]

$$P_C = \frac{J_{ph}}{J_{ph,sat}}. \quad (2)$$

As can be seen in Fig. S14 (ESI†), the PTB7-Th:CETIC-4F and PTB7-Th:COTIC-4F devices exhibit a better charge collection P_C than their PBDBT counterparts. When the two NFAs are compared, PTB7-Th:CETIC-4F and PBDBT:CETIC-4F devices show a higher P_C than PTB7-Th:COTIC-4F and PBDBT:COTIC-4F devices, respectively; this difference is subtle for the PTB7-Th devices, while significant for the PBDBT devices. Ultimately, a reasonable correlation between the collection probability P_C and the device performance can be observed, where higher values for P_C, specifically at forward bias around maximum-power conditions, go hand in hand with higher values for the solar cell PCEs. Additionally, *J*–*V*-curves at varying light intensities were measured to qualitatively inspect the non-geminate recombination mechanisms (Fig. S15, ESI†). The light intensities were decreased by neutral density filters. Commonly, the relationship between the J_{SC} and the light intensity I follows a power law ($J_{SC} \propto I^{\alpha}$), where the value of the exponent α indicates the presence of bimolecular recombination ($\alpha \to 0.5$) and/or space charge effects caused by differences in hole and electron mobility ($\alpha \to 0.75$). In the case of the studied blends similar values for the exponent ($\alpha \approx 0.9$) were determined.[30,31] Indeed, the hole and electron mobility ($\mu_{h,e}$) obtained *via* single-carrier diodes analyzed *via* the Mott-Gurney relationship show significant differences in the magnitude of the two types of mobility for all systems (μ_h/μ_e = 5–138, Fig. S18 and Table S2, ESI†). It is therefore likely that the deviation of the exponent α from unity is caused by the aforementioned space charge effect rather than by the influence of bimolecular recombination alone. The second common approach to investigate the types of non-geminate recombination mechanisms of solar cells is by determining the relationship between the V_{OC} and the light intensity I:[32,33]

$$V_{OC} \propto \frac{kT}{q} \ln(I), \quad (3)$$

where k is the Boltzmann constant, T is the absolute temperature (T = 300 K), and q is the elementary charge.[34] The V_{OC}–ln(I)-plots exhibit a slope of $S = 1kT/q$ for solar cells in the case of ideal, pure bimolecular recombination. However, the presence of bulk or surface traps can cause monomolecular

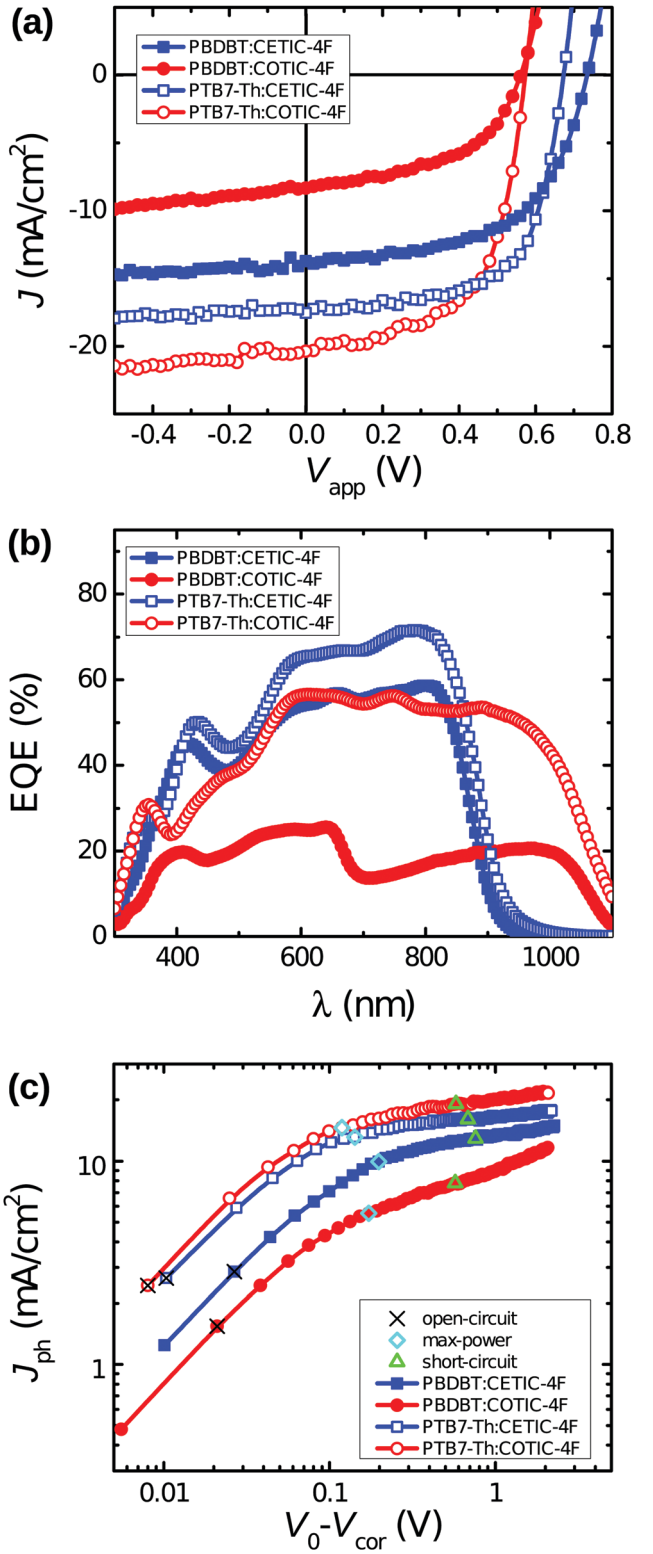

Fig. 2 (a) *J*–*V*-characteristics, (b) EQE, and (c) photocurrent density J_{ph} as a function of the effective voltage V_0–V_{cor} of the studied solar cells. Operating conditions of interest such as open-circuit, max-power, and short-circuit are highlighted for convenience.

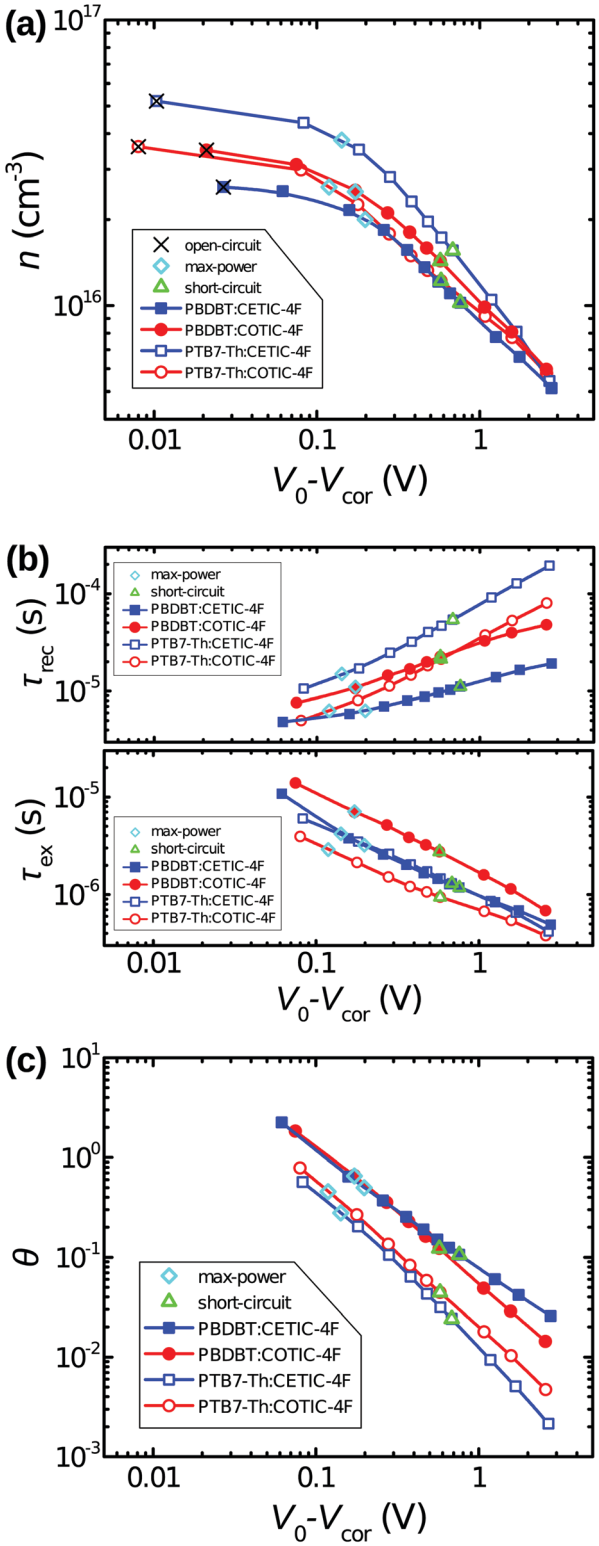

Fig. 3 (a) Charge carrier density n, (b) recombination lifetime τ_{rec} as well as extraction time τ_{ex}, and (c) competition factor θ as a function of the effective voltage V_0–V_{cor} of the studied solar cell determined *via* capacitance spectroscopy. Operating conditions of interest such as max-power, and short-circuit are highlighted for convenience.

recombination that lead to deviations of the slope (bulk traps: $S > 1kT/q$; surface traps: $S < 1kT/q$).[22,35,36] The V_{OC}–ln(I)-plots exhibit good linearity over the investigated light intensities and the slopes determined for the studied devices are in a range of S = 0.84–1.13kT/q. These results indicate that all types of non-geminate recombination should be taken into account as loss mechanisms.[36] Hence, the light intensity dependent J–V-curves are not sufficient to paint a conclusive picture of the non-geminate recombination dynamics and a more in-depth analysis is necessary to obtain quantitative results.

The recombination dynamics in the studied solar cells were quantified *via* an analysis based on capacitance spectroscopy that allows the determination of the charge carrier density n (eqn (S3)–(S5), Fig. S19, ESI† Fig. 3a).[37] The studied solar cells show charge carrier densities in a similar range, with the biggest divergence at forward bias approaching open-circuit conditions (highest for PTB7-Th:CETIC-4F: $n = 5.2 \times 10^{16}$ cm^{-3}; lowest for PBDBT:CETIC-4F: $n = 2.6 \times 10^{16}$ cm^{-3}). To obtain a quantitative understanding of the recombination mechanisms, it is assumed that the overall measured recombination current density ($J_{rec} = J_{ph,sat} - J_{ph}$) is a superposition of the three aforementioned recombination mechanisms that contribute a certain part to the total recombination current density J_{rec}:

$$J_{rec} = J_{bm} + J_{tb} + J_{ts} = qL\left(\frac{n}{\tau_{bm}} + \frac{n}{\tau_{tb}} + \frac{n}{\tau_{ts}}\right) = qL\left(k_{bm}n^2 + k_{tb}n + k_{ts}n\right), \quad (4)$$

where q is the elementary charge, L is the active layer thickness, τ is the charge carrier lifetime, n is the charge carrier density, and k is the recombination coefficient of the three different recombination mechanisms (bm: bimolecular; tb: bulk trap-assisted; ts: surface trap-assisted). By reconstructing the recombination current density J_{rec} obtained from the J–V-curves with the charge carrier density (n) and the effective mobility (μ_{eff}), which is explained in the ESI,† it is possible to quantify the recombination coefficients (k) (Fig. S20–S22, ESI†).[22,38] In general, the PTB7-Th:COTIC-4F and PBDBT:COTIC-4F devices exhibit higher bimolecular recombination coefficients k_{bm} than their CETIC-4F-based counterparts. Furthermore, the fitting yields higher contributions of bulk trap-assisted recombination in the PBDBT:CETIC-4F and PBDBT:COTIC-4F devices compared to the PTB7-Th:CETIC-4F and PTB7-Th:COTIC-4F solar cells, which could be the reason for the reduced performance of the PBDBT OSCs (Fig. S22, ESI†). In addition, the contributions of surface trap-assisted recombination are only relevant under open-circuit conditions for all tested devices and even under these conditions they do not dominate the non-geminate recombination dynamics (Fig. S21, ESI†).

In a subsequent step, it is possible to calculate the charge carrier lifetime τ_{rec} by rearranging eqn (4), since the carrier density n and the relevant recombination coefficients (k_{bm}, k_{tb}, k_{ts}) are now known (Fig. 3b). However, it is necessary to also take the extraction dynamics of the investigated solar cells into account to obtain a complete picture, since non-geminate recombination and extraction are in a direct competition to each

Table 1 Photovoltaic performance of OSCs with blends consisting of PBDBT or PTB7-Th as donor and CETIC-4F and COTIC-4F as acceptor, measured at simulated 100 mW cm^{-2} AM 1.5G illumination

Donor	NFA	V_{OC} [V]	J_{SC} [mA cm^{-2}]	FF	$PCE_{avg(max)}$ [%]	$J_{SC,calc}$ [mA cm^{-2}]	EQE_{max} [%]
PBDBT[a]	CETIC-4F	0.71 ± 0.01	15.6 ± 1.1	0.54 ± 0.03	5.96 ± 0.77 (6.59)	15.72	58
	COTIC-4F	0.55 ± 0.03	8.0 ± 0.3	0.49 ± 0.01	2.19 ± 0.12 (2.32)	7.78	26
PTB7-Th[b]	CETIC-4F	0.65 ± 0.01	19.1 ± 1.0	0.61 ± 0.03	7.61 ± 0.33 (8.08)	18.66	72
	COTIC-4F	0.56 ± 0.01	20.2 ± 0.9	0.59 ± 0.01	6.66 ± 0.17 (7.04)	20.40	57

[a] PBDBT : NFA blend ratio: 1 : 1 (w/w). [b] PTB7-Th : NFA blend ratio: 1 : 1.5 (w/w). [c] Average values from 10 devices. [d] J_{SC} calculated from EQE measurements.

other (see eqn (S6)–(S8), ESI†).[21,39] To this end, the effective extraction time τ_{ex} can be defined as follows:

$$\tau_{ex} = \frac{qLn}{J}, \quad (5)$$

where q is the elementary charge, L is the active layer thickness, n is the charge carrier density, and J is the current density (Fig. 3b).[38] Once the charge carrier lifetime and the extraction time are determined, it is possible to calculate the competition factor ($\theta = \tau_{ex}/\tau_{rec}$), a figure of merit introduced by Barthesaghi *et al.* in 2015.[39] In this study, the bias-dependent competition factor θ is accessible, since the bias-dependent lifetime and extraction time were determined.[38] In summary, a good reciprocal relationship between the competition factor θ and figures of merit for the device performance (FF, PCE) can be observed (Table 2), where lower θ values go hand in hand with a higher device performance.

In addition to the analysis based on capacitance spectroscopy, we also performed transient open-circuit voltage decay measurements on the solar cells as a secondary method to investigate the relevant non-geminate recombination processes (see eqn (S9)–(S14) and Fig. S23, ESI†). The V_{OC}-transients depicted convey significant differences between the PTB7-Th and PBDBT devices (Fig. 4a). It takes up to one order of magnitude longer for the V_{OC} to drop to half of its initial value for PTB7-Th:CETIC-4F and PTB7-Th:COTIC-4F devices ($t_{1/2}$ = 0.6–1.2 ms), when compared to their PBDBT:CETIC-4F and PBDBT:COTIC-4F counterparts ($t_{1/2}$ = 0.06–0.13 ms; Table 2), which is suggestive of higher recombination rates in the PBDBT devices. The carrier lifetime τ_{rec} and the recombination order β can be determined from the transients of the V_{OC} for the relevant timescales not dominated by the shunt resistance limit (PTB7-Th devices: $t < 10^{-3}$ s; PBDBT devices: $t < 10^{-4}$ s, Fig. S23, ESI†). It is revealed that the highest recombination order β_{max} reached for the PTB7-Th:CETIC-4F and PTB7-Th:COTIC-4F devices ($\beta_{max} \approx 1.6$) is larger than for the PBDBT:CETIC-4F and PBDBT:COTIC-4F devices ($\beta_{max} \approx 1.4$) (eqn (S11)–(S14), Fig. S23, ESI,† and Table 2). Another interpretation of the recombination order β is as an indicator of the relative contribution to the effective recombination by bimolecular and/or monomolecular recombination.[40] Therefore, higher values of β_{max} result either from an increased bimolecular contribution, a decreased trap-assisted (e.g. monomolecular) contribution, or a combination of both cases. To fully quantify the recombination, it is necessary to transform the measured V_{OC} values to the transient charge carrier density n_{OC} and plot the carrier lifetime τ_{rec} against it (Fig. 4b and c). Furthermore, it has to be stressed that bulk and surface trap-assisted recombination cannot be distinguished by this method.[22] The analysis to obtain the transient carrier density n_{OC} and the lifetime τ is described in detail in the ESI† (eqn (S11)–(S14)). In essence the carrier densities under open-circuit conditions determined *via* capacitance spectroscopy act as a reference point for the transformation of the transient V_{OC} to the transient n_{OC} values.[11,22] Finally, it is possible to obtain values for the different recombination coefficients k_{bm} and k_t (bm: bimolecular; t: trap-assisted) by fitting the relevant parts of the measured charge carrier lifetime τ (*i.e.* at high levels of excitation). All studied devices exhibit some bimolecular and trap-assisted recombination, which is evidenced by the respective recombination coefficients (Table 2).[22] In general, PTB7-Th:COTIC-4F and PBDBT:COTIC-4F devices exhibit the highest bimolecular recombination coefficients ($k_{bm} \approx 2.0 \times 10^{-11}$ cm^3 s^{-1}), while PTB7-Th:CETIC-4F and PBDBT:CETIC-4F devices show values in a smaller range ($k_{bm} \approx (0.6–1.4) \times 10^{-11}$ cm^3 s^{-1}). The magnitude of k_{bm} is inversely proportional to the bandgap of the studied blend system, which correlates with the results obtained *via* capacitance spectroscopy and is in agreement with what would be expected from the fundamental relationships governing bimolecular recombination.[41] In the case of trap-assisted recombination, PBDBT:CETIC-4F and PBDBT:COTIC-4F devices show nearly two orders of magnitude higher values for the relevant recombination coefficient ($k_t \approx 10^5$ s^{-1}), than the respective PTB7-Th:NFA OSCs ($k_t \approx 10^3$ s^{-1}).

The investigation of the morphology suggests that the order in the blend films could be responsible for the differences in trap-assisted recombination and ultimately performance that were

Table 2 Recombination dynamics of OSCs with blends consisting of PBDBT or PTB7-Th as donor and CETIC-4F and COTIC-4F as acceptor

Donor	NFA	FF	PCE_{max} [%]	θ_{SC}	θ_{MP}	$t_{1/2}$ [ms]	β_{max}	k_{bm} [cm^3 s^{-1}]	k_t [s^{-1}]
PBDBT	CETIC-4F	0.54	6.59	0.1060	0.4997	0.13	1.4	$(0.60 \pm 0.02) \times 10^{-11}$	$(9.92 \pm 0.12) \times 10^4$
	COTIC-4F	0.49	2.32	0.1226	0.6544	0.06	1.4	$(2.15 \pm 0.05) \times 10^{-11}$	$(9.83 \pm 0.19) \times 10^4$
PTB7-Th	CETIC-4F	0.61	8.08	0.0241	0.2778	1.20	1.6	$(1.35 \pm 0.02) \times 10^{-11}$	$(1.66 \pm 0.07) \times 10^3$
	COTIC-4F	0.59	7.04	0.0444	0.4552	0.60	1.7	$(2.06 \pm 0.09) \times 10^{-11}$	$(1.54 \pm 0.16) \times 10^3$

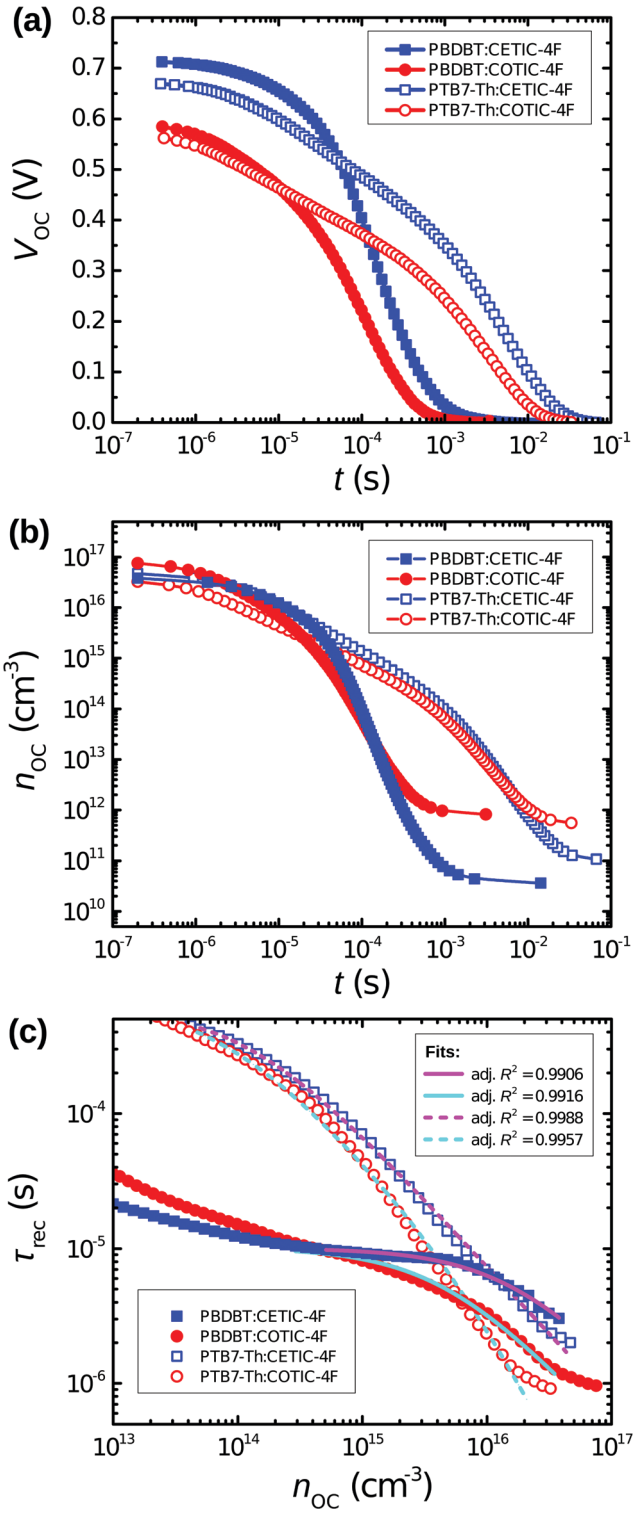

Fig. 4 (a) Transients of open-circuit voltage V_{OC} and (b) open-circuit carrier density n_{OC} of the studied solar cells. (c) Charge carrier lifetime τ_{rec} *vs.* the transient open-circuit carrier density n_{OC} and their corresponding fits determined *via* open-circuit voltage decay.

observed for devices with the two studied donor materials. In particular, the PBDBT:CETIC-4F and PBDBT:COTIC-4F blends show less order in comparison to the PTB7-Th:CETIC-4F and PTB7-Th:COTIC-4F blends, as evidenced by GIWAXS and AFM measurements (Fig. S24 and S25, ESI†). The roughness in the AFM measurements is consistently higher for PBDBT:CETIC-4F and PBDBT:COTIC-4F blends than for the PTB7-Th:CETIC-4F and PTB7-Th:COTIC-4F blends. GIWAXS measurements show that there are diffraction peaks from the donor and the acceptor component in the PTB7-Th:CETIC-4F and PTB7-Th:COTIC-4F blends, while the scattering from PBDBT:CETIC-4F and PBDBT:COTIC-4F blends is dominated by the polymer. The difference in film composition (60% NFA in PTB7-Th blends and 50% NFA in PBDBT blends) is not likely to account for such a dramatic difference. This suggests that the NFA domain is significantly less ordered in blends with PBDBT than with PTB7-Th.

Our results show that the difference in trap-assisted recombination is related to whether PTB7-Th or PBDBT is being used as the donor component of the blend, whereas the difference in bimolecular recombination is related to the magnitude of the bandgap.

Future studies may focus on elucidating how the side chains influence the crystallinity, phonon coupling, and the resulting photophysical recombination processes. A combination of theoretical calculations and experiments such as advanced X-ray scattering, Raman spectroscopy and neutron scattering would be necessary to uncover these underlying mechanisms.

3. Conclusion

In conclusion, the synthesis and characterization of the new NFA CETIC-4F is described and it was shown that altering the sub-donor (D′) fragments is a viable strategy to finely tune the energy levels. The performance of solar cells based on the common polymer donors PTB7-Th and PBDBT, as well as the systematically structurally modified NFAs CETIC-4F and COTIC-4F are investigated. The solar cells exhibited charge generation at wide spectral ranges (300–950 nm), reaching wavelengths as long as 1100 nm in the case of PBDBT:COTIC-4F and PTB7-Th:COTIC-4F. The PCEs achieved for PTB7-Th:CETIC-4F and PTB7-Th:COTIC-4F devices (8%, and 7%, respectively) were consistently higher than for devices employing PBDBT:CETIC-4F and PBDBT:COTIC-4F (6%, and 2%, respectively). This observation could be linked to considerably higher monomolecular, *i.e.*, bulk trap-assisted recombination losses for the PBDBT:CETIC-4F and PBDBT:COTIC-4F devices that were determined *via* analyses based on capacitance spectroscopy and open-circuit voltage decay measurements. AFM and GIWAXS results indicate that the PBDBT:NFA blend films show higher roughness and less order in contrast to the PTB7-Th:NFA blends, which likely cause the increased trap-assisted recombination. Furthermore, PTB7-Th:COTIC-4F and PBDBT:COTIC-4F devices exhibited higher bimolecular recombination coefficients than their PTB7-Th:CETIC-4F and PBDBT:CETIC-4F counterparts, which is in agreement with what would be expected from the fundamental, inverse relationship between the bandgap and bimolecular recombination.

Conflicts of interest

There are no conflicts to declare.

Acknowledgements

J. V., J. L., and S.-J. K. contributed equally to this work. J. V. acknowledges primary funding by the Alexander-von-Humboldt Stiftung. J. V., V. B., S.-J. K. and T.-Q. N. acknowledge funding by the Office of Naval Research (ONR) grant #N000141410076. J. L. acknowledges funding by the Center for Advanced Soft Electronics under the Global Frontier Research Program (code no. 2011-0031628) of the Ministry of Science and ICT, Korea. X-ray scattering experiments were carried out at the Advanced Light Source, which is a DOE Office of Science user facility under contract no. DE-AC02-05CH11231. We thank Dr Alexander Mikhailovsky and Ben R. Luginbuhl for assistance with building and testing the measurement setup used for V_{OC}-decay as well as Jianfei Huang, Sangcheol Yoon, Nora Schopp, Tung Dang Nguyen, Alana Dixon, Álvaro Daniel Romero-Borja, Alexander Lill, Brett Yurash, David Cao and Zhifang Du for fruitful discussions. This paper is dedicated to Professor Tobin Marks on the occasion of his 75th birthday.

References

1 G. Yu, J. Gao, J. C. Hummelen, F. Wudl and A. J. Heeger, Polymer photovoltaic cells: enhanced efficiencies *via* a network of internal donor–acceptor heterojunctions, *Science*, 1995, **270**(5243), 1789–1791.

2 L. Lu, T. Zheng, Q. Wu, A. M. Schneider, D. Zhao and L. Yu, Recent advances in bulk heterojunction polymer solar cells, *Chem. Rev.*, 2015, **115**(23), 12666–12731.

3 C. Li and H. Wonneberger, Perylene imides for organic photovoltaics: yesterday, today, and tomorrow, *Adv. Mater.*, 2012, **24**(5), 613–636.

4 G. Zhang, J. Zhao, P. C. Y. Chow, K. Jiang, J. Zhang, Z. Zhu, J. Zhang, F. Huang and H. Yan, Nonfullerene acceptor molecules for bulk heterojunction organic solar cells, *Chem. Rev.*, 2018, **118**(7), 3447–3507.

5 J. Zhao, Y. Li, G. Yang, K. Jiang, H. Lin, H. Ade, W. Ma and H. Yan, Efficient organic solar cells processed from hydrocarbon solvents, *Nat. Energy*, 2016, **1**(2), 15027.

6 Y. Jin, Z. Chen, M. Xiao, J. Peng, B. Fan, L. Ying, G. Zhang, X.-F. Jiang, Q. Yin, Z. Liang, F. Huang and Y. Cao, Thick film polymer solar cells based on naphtho [1,2-*c*: 5,6-*c*] bis[1,2,5] thiadiazole conjugated polymers with efficiency over 11%, *Adv. Energy Mater.*, 2017, **7**(22), 1700944.

7 L. Meng, Y. Zhang, X. Wan, C. Li, X. Zhang, Y. Wang, X. Ke, Z. Xiao, L. Ding, R. Xia, H.-L. Yip, Y. Cao and Y. Chen, Organic and solution-processed tandem solar cells with 17.3% efficiency, *Science*, 2018, **361**(6407), 1094–1098.

8 N. Gasparini, A. Salleo, I. McCulloch and D. Baran, The role of the third component in ternary organic solar cells, *Nat. Rev. Mater.*, 2019, **4**, 229–242.

9 Y. Cui, H. Yao, J. Zhang, K. Xian, T. Zhang, L. Hong, Y. Wang, Y. Xu, K. Ma, C. An, C. He, Z. Wei, F. Gao and Jianhui Hou, Single-junction organic photovoltaic cells with approaching 18% efficiency, *Adv. Mater.*, 2020, 1908205.

10 J. Huang, J. Lee, J. Vollbrecht, V. V. Brus, A. L. Dixon, D. X. Cao, Z. Zhu, Z. Du, H. Wang and K. Cho, *et al.*, A high-performance solution-processed organic photodetector for near-infrared sensing, *Adv. Mater.*, 2019, **32**(1), 1906027.

11 J. Lee, S.-J. Ko, H. Lee, J. Huang, Z. Zhu, M. Seifrid, J. Vollbrecht, V. V. Brus, A. Karki and H. Wang, *et al.*, Side chain engineering of non-fullerene acceptors for near-infrared organic photodetectors and photovoltaics, *ACS Energy Lett.*, 2019, **4**(6), 1401–1409.

12 R. R. Lunt and V. Bulovic, Transparent, near-infrared organic photovoltaic solar cells for window and energy-scavenging applications, *Appl. Phys. Lett.*, 2011, **98**(11), 61.

13 V. V. Brus, J. Lee, B. Luginbuhl, S.-J. Ko, G. C. Bazan and T.-Q. Nguyen, Solution-processed semitransparent organic photovoltaics: from molecular design to device performance, *Adv. Mater.*, 2019, **31**(30), 1900904.

14 M. Azzouzi, J. Yan, T. Kirchartz, K. Liu, J. Wang, H. Wu and J. Nelson, Nonradiative energy losses in bulk-heterojunction organic photovoltaics, *Phys. Rev. X*, 2018, **8**(3), 031055.

15 M. S. Vezie, M. Azzouzi, A. M. Telford, T. R. Hopper, A. B. Sieval, J. C. Hummelen, K. Fallon, H. Bronstein, Thomas Kirchartz and Ahomas Ahomas Bakulin, *et al.*, Impact of marginal exciton–charge-transfer state offset on charge generation and recombination in polymer: fullerene solar cells, *ACS Energy Lett.*, 2019, **4**(9), 2096–2103.

16 H. Cha, S. Wheeler, S. Holliday, S. D. Dimitrov, A. Wadsworth, H. H. Lee, D. Baran, I. McCulloch and J. R. Durrant, Influence of blend morphology and energetics on charge separation and recombination dynamics in organic solar cells incorporating a nonfullerene acceptor, *Adv. Funct. Mater.*, 2018, **28**(3), 1704389.

17 C.-H. Tan, J. Gorman, A. Wadsworth, S. Holliday, S. Subramaniyan, S. A. Jenekhe, D. Baran, I. McCulloch and J. R. Durrant, Barbiturate end-capped non-fullerene acceptors for organic solar cells: tuning acceptor energetics to suppress geminate recombination losses, *Chem. Commun.*, 2018, **54**(24), 2966–2969.

18 D. Baran, N. Gasparini, A. Wadsworth, C. H. Tan, N. Wehbe, X. Song, Z. Hamid, W. Zhang, M. Neophytou, T. Kirchartz, C. J. Brabec, J. R. Durrant and I. McCulloch, Robust non-fullerene solar cells approaching unity external quantum efficiency enabled by suppression of geminate recombination, *Nat. Commun.*, 2018, **9**(1), 1–9.

19 Z. He, B. Xiao, F. Liu, H. Wu, Y. Yang, S. Xiao, C. Wang, T. P. Russell and Y. Cao, Single-junction polymer solar cells with high efficiency and photovoltage, *Nat. Photonics*, 2015, **9**(3), 174.

20 D. Qian, L. Ye, M. Zhang, Y. Liang, L. Li, Y. Huang, X. Guo, S. Zhang, Z. Tan and J. Hou, Design, application, and morphology study of a new photovoltaic polymer with strong aggregation in solution state, *Macromolecules*, 2012, **45**(24), 9611–9617.

21 M. C. Heiber, T. Okubo, S.-J. Ko, B. R. Luginbuhl, N. Ran, M. Wang, H. Wang, M. A. Uddin, H. Y. Woo and G. C. Bazan, *et al.*, Measuring the competition between bimolecular

charge recombination and charge transport in organic solar cells under operating conditions, *Energy Environ. Sci.*, 2018, **11**, 3019–3032.

22 J. Vollbrecht, V. V. Brus, S.-J. Ko, J. Lee, A. Karki, D. X. Cao, K. Cho, G. C. Bazan and T.-Q. Nguyen, Quantifying the nongeminate recombination dynamics in nonfullerene bulk heterojunction organic solar cells, *Adv. Energy Mater.*, 2019, **9**(32), 1901438.

23 J. Lee, S.-J. Ko, M. Seifrid, H. Lee, B. R. Luginbuhl, A. Karki, M. Ford, K. Rosenthal, K. Cho and T.-Q. Nguyen, *et al.*, Bandgap narrowing in non-fullerene acceptors: single atom substitution leads to high optoelectronic response beyond 1000 nm, *Adv. Energy Mater.*, 2018, **8**(24), 1801212.

24 M. Zhang, X. Guo, W. Ma, H. Ade and J. Hou, A polythiophene derivative with superior properties for practical application in polymer solar cells, *Adv. Mater.*, 2014, **26**(33), 5880–5885.

25 L. Huo, Y. Zhou and Y. Li, Alkylthio-substituted polythiophene: absorption and photovoltaic properties, *Macromol. Rapid Commun.*, 2009, **30**(11), 925–931.

26 A. Karki, G.-J. A. H. Wetzelaer, G. N. M. Reddy, V. Nádaždy, M. Seifrid, F. Schauer, G. C. Bazan, B. F. Chmelka, P. W. M. Blom and T.-Q. Nguyen, Unifying energetic disorder from charge transport and band bending in organic semiconductors, *Adv. Funct. Mater.*, 2019, **29**(20), 1901109.

27 V. V. Brus, C. M. Proctor, N. A. Ran and T.-Q. Nguyen, Capacitance spectroscopy for quantifying recombination losses in nonfullerene small-molecule bulk heterojunction solar cells, *Adv. Energy Mater.*, 2016, **6**(11), 1502250.

28 J. Vollbrecht, C. Wiebeler, H. Bock, S. Schumacher and H.-S. Kitzerow, Curved polar dibenzocoronene esters and imides *versus* their planar centrosymmetric homologs: photophysical and optoelectronic analysis, *J. Phys. Chem. C*, 2019, **123**, 4483–4492.

29 A. K. Ko Kyaw, D. H. Wang, D. Wynands, J. Zhang, T.-Q. Nguyen, G. C. Bazan and A. J. Heeger, Improved light harvesting and improved efficiency by insertion of an optical spacer (zno) in solution-processed small-molecule solar cells, *Nano Lett.*, 2013, **13**(8), 3796–3801.

30 S. R. Cowan, N. Banerji, W. L. Leong and A. J. Heeger, Charge formation, recombination, and sweep-out dynamics in organic solar cells, *Adv. Funct. Mater.*, 2012, **22**(6), 1116–1128.

31 L. J. A. Koster, V. D. Mihailetchi, H. Xie and P. W. M. Blom, Origin of the light intensity dependence of the short-circuit current of polymer/fullerene solar cells, *Appl. Phys. Lett.*, 2005, **87**(20), 203502.

32 C. M. Proctor, M. Kuik and T.-Q. Nguyen, Charge carrier recombination in organic solar cells, *Prog. Polym. Sci.*, 2013, **38**(12), 1941–1960.

33 M. Azzouzi, T. Kirchartz and J. Nelson, Factors controlling open-circuit voltage losses in organic solar cells, *Trends Chem.*, 2019, **1**(1), 49–62.

34 L. Jan, A. Koster, V. D. Mihailetchi, R. Ramaker and P. W. M. Blom, Light intensity dependence of open-circuit voltage of polymer: fullerene solar cells, *Appl. Phys. Lett.*, 2005, **86**(12), 123509.

35 M. M. Mandoc, F. B. Kooistra, J. C. Hummelen, B. De Boer and P. W. M. Blom, Effect of traps on the performance of bulk heterojunction organic solar cells, *Appl. Phys. Lett.*, 2007, **91**(26), 263505.

36 V. V. Brus, Light dependent open-circuit voltage of organic bulk heterojunction solar cells in the presence of surface recombination, *Org. Electron.*, 2016, **29**, 1–6.

37 C. M. Proctor, C. Kim, D. Neher and T.-Q. Nguyen, Nongeminate recombination and charge transport limitations in diketopyrrolopyrrole-based solution-processed small molecule solar cells, *Adv. Funct. Mater.*, 2013, **23**(28), 3584–3594.

38 A. Karki, J. Vollbrecht, A. L. Dixon, N. Schopp, M. Schrock, G. N. Manjunatha Reddy and T.-Q. Nguyen, Understanding the high performance of over 15% efficiency in single-junction bulk heterojunction organic solar cells, *Adv. Mater.*, 2019, **31**(48), 1903868.

39 D. Bartesaghi, I. del Carmen Pérez, J. Kniepert, S. Roland, M. Turbiez, D. Neher and L. Jan Anton Koster, Competition between recombination and extraction of free charges determines the fill factor of organic solar cells, *Nat. Commun.*, 2015, **6**, 7083.

40 V. V. Brus, F. Lang, J. Bundesmann, S. Seidel, A. Denker, B. Rech, G. Landi, H. C. Neitzert, J. Rappich and N. H. Nickel, Defect dynamics in proton irradiated ch3nh3pbi3 perovskite solar cells, *Adv. Electron. Mater.*, 2017, **3**(2), 1600438.

41 W. Van Roosbroeck and W. Shockley, Photon-radiative recombination of electrons and holes in germanium, *Phys. Rev.*, 1954, **94**(6), 1558.

